Numerical investigation into the influence on hydrofoil vibrations of water tunnel test section acoustic modes

Wei Wang

College of Water Resources and Civil Engineering, China Agricultural University,
Beijing 100083, China
1943459226@qq.com

Lingjiu Zhou*

College of Water Resources and Civil Engineering, China Agricultural University,
Beijing Engineering Research Centre of Safety and Energy Saving Technology for Water
Supply Network System
Beijing 100083, China
zlj@cau.edu.cn

Zhengwei Wang

Department of Thermal Engineering, Tsinghua University,
Beijing 100084, China
wzw@mail.tsinghua.edu.cn

Xavier Escaler

Department of Fluid Mechanics, Universitat Politècnica de Catalunya-Barcelona Tech,
Barcelona 08028, Spain
xavier.escaler@upc.edu

Oscar De La Torre

School of Marine Science and Engineering, Plymouth University,
Plymouth PL4 8AA, United Kingdom
oscar.delatorre@plymouth.ac.uk

VIB-18-1397, Corresponding author: Zhou

ABSTRACT

High-speed water tunnels are typically used to investigate the single phase and two-phase flows around hydrofoils for hydraulic machinery applications but their dynamic behavior is not usually evaluated. The modal analysis of a NACA0009 hydrofoil inside the test section were calculated with a coupled acoustic fluid-structure, which shows a good agreement with the experimental results. This numerical model has been used to study the influence on the hydrofoil modes of vibration of the acoustic properties of the surrounding fluid and of the tunnel test section dimensions. It has been found that the natural frequencies of the acoustic domain are inversely proportional to the test section dimensions. Moreover, these acoustic frequencies decrease linearly with the reduction of the speed of sound in the fluid medium. However, the hydrofoil frequencies are not affected by the change of the speed of sound except when they match an acoustic frequency. If both mode shapes are similar, a strong coupling occurs and the hydrofoil vibration follows the linear reduction of natural frequency induced by the acoustic mode. If both mode shapes are dissimilar, a new mode appears whose frequency decreases linearly with speed of sound while keeping the acoustic mode of vibration. This new fluid-structure mode of vibration appears in between two hydrofoil structure modes and its evolution with sound speed reduction has been called "mode transition". Overall, these findings reinforce the idea that fluid-structure interaction effects must be taken into account when studying the induced vibrations on hydrofoils inside water tunnels.

Keywords: *hydrofoil; fluid-structure interaction; natural frequencies; structure modes; acoustic modes; coupling types, speed of sound.*

1 Introduction

Surrounding water has a great influence on the dynamic behaviour of submerged structures due to the added mass effect as demonstrated by Lindholm et al. [1] who compared the vibrations of cantilever plates in air and water. Meyerhoff [2] used a dipole distribution upon the plates to compute unsteady-pressure distributions and added mass of thin rectangular plates. Kwak [3] studied the effect of fluid on the natural frequencies of circular plates and obtained the ratio between the natural frequencies in fluid and the natural frequencies in air due to the increase of inertia. Later, Amabili [4] calculated the natural frequencies and mode shapes of circular and annular plates by using a Galerkin equation minimizing the Rayleigh quotient. Chang and Liu [5] determined experimentally the mode shapes of a plate in a flow and reported small changes relative to the air condition. Rodriguez et al. [6] carried out similar experimental investigations with a Francis turbine runner by using experimental modal analysis. They found that the mode shapes in water were similar to those in air but with lower natural frequencies and higher damping ratios. Valentín et al. [7] used three different liquids to evaluate the influence of fluid viscosity and density on the natural frequencies of a confined disk attached to a shaft inside a cylindrical container. Escaler and De La Torre [8] carried out experimental and numerical analyses to determine the effects of water loading on the axisymmetric modes of vibration of a circular plate. They found that measurable differences existed in the mode shapes between corresponding dry and wet modes due to fluid-structure coupling.

The acoustic properties of the enclosed fluid around a solid body may also have a major influence on the fluid-structure system response as found by Parker [9] from the experimental observations of plate vibrations induced by the vortex shedding in air. He found out that under certain conditions system resonances can be caused by purely acoustic effects which are

unrelated to the mechanical vibrations of the plate. Later, Parker et al. [10-11] observed the amplitude of a cantilever plate forced vibration excited by an acoustic resonance was larger than the amplitude induced by a mechanical resonance. In fact, significant amplitudes were generated in the system when there was a significant degree of coupling between the mechanical and the acoustic resonances. This "Parker-type modes" was also reported by many other authors, such as Woodley and Peake [12], Bardakhanov [13] and Konig [14], who confirmed that the acoustic modes have an important influence on the structural vibration.

Recently, Bossio et al. [15] recently studied the dynamic response of a submerged disk for different values of the acoustic natural frequencies of the fluid cavity. To do so, they modified the geometrical parameters of the cavity as well as the fluid speed of sound. These parameters influence the values of the acoustic natural frequencies as found by Blevins [16]. In particular, they found that the disk modes of vibration could be considerably affected when the value of the speed of sound was decreased because, then, the acoustic natural frequencies were also reduced and they approached the disk natural frequencies. Meanwhile, Liu et al. [21] found that a transition mode appeared with the change of sound speed in the cavity.

Under certain circumstances it might be possible that the speed of sound deviates significantly from the pure water conditions. This is the case when a two-phase flow exists around the submerged structure. As it can be seen in Figure 1 taken from Brennen [17], the void ratio, that is the fraction of the volume occupied by the gas phase, modifies drastically the sound speed through a bubbly air/water mixture. For example, typical gas-liquid two-phase flows can take place in chemical pumps that transport volatile liquids, as wall as in the extraction and transportation processes in the petroleum industry and inside water turbines under cavitation conditions. Nevertheless, these effects have not been deeply addressed yet.

Based on the previous considerations, the aim of the present study has been to evaluate

the influence of the acoustic modes on the natural frequencies and mode shapes of a 2D hydrofoil located in a high-speed water tunnel test section. For that, the experimental and the numerical studies carried out by de la Torre et al. [18-20] for a cantilevered NACA0009 hydrofoil surrounded by still water have been considered. The fluid-structure interaction (FSI) phenomena have been modelled with a coupled Acoustic Fluid-Structural model described in Section 2. The accuracy of the model has been checked in Section 3 against experimental results obtained under both air and still water conditions. Then, the prediction of hydrofoil modes induced by acoustic modes of the test section has been described in Section 4. Next, the model has been modified to study the influence of both the test section dimensions and of the speed of sound on the coupled modes as described in Sections 5 and 6. Finally, the conclusions have been presented in Section 7.

2 Coupled acoustic fluid-structure model

The coupled fluid-structure system developed with ANSYS Workbench® version 12.0 can be written as:

$$[M_s]\{\ddot{u}\} + [C_s]\{\dot{u}\} + [K_s]\{u\} = \{F_s\} + \{F_{fs}\} \tag{1}$$

$$[M_f]\{\ddot{p}\} + [C_f]\{\dot{p}\} + [K_f]\{p\} = \{F_f\} + \{F_{sf}\} \tag{2}$$

where, $[M_s]$ is the structural mass matrix, $[C_s]$ is the structural damping matrix, $[K_s]$ is the structural stiffness matrix, $\{F_s\}$ is the structure load vector, $\{F_{fs}\}$ is the force that the fluid exerts on the structure, and $\{u\}$ is the nodal displacement vector. $[M_f]$ is the acoustic mass matrix, $[C_f]$ is the acoustic fluid damping matrix, $[K_f]$ is the acoustic fluid stiffness matrix, $\{F_f\}$ is the acoustic fluid load vector, $\{F_{sf}\}$ is the force that the structure motion produces on the fluid, and $\{p\}$ is the nodal pressure vector.

For modal analysis, it can be assumed that $[C_s] = 0$, $[C_f] = 0$, $\{F_s\} = 0$ and $\{F_f\} = 0$, and then the following coupled equations can be solved:

$$\left[-[M_s]\omega^2 + [K_s]\right]\{u\} = [R]\{p\} \tag{3}$$

$$\left[-[M_f]\omega^2 + [K_f]\right]\{p\} = \rho_0 [R]^T \omega^2 \{u\} \tag{4}$$

where, ω is the frequency, $[R]$ is the acoustic fluid boundary matrix and ρ_0 is the acoustic fluid density constant.

For convenience in the following analysis, the acoustic fluid mass matrix is developed as follows:

$$[M_f] = \frac{1}{c_f^2} \iiint_{\Omega_F} \{N_p\}\{N_p\}^T dv = \frac{1}{c_f^2}[\bar{M}_f] \tag{5}$$

where $\{N_p\}$ is element shape function for pressure, c_f is the speed of sound in the fluid medium, dv is differential volume and Ω_F is the total fluid volume. Then, substituting Equation (5) into Equation (4) we obtain:

$$\left[-\frac{1}{c_f^2}[\bar{M}_f]\omega^2 + [K_f]\right]\{p\} = \rho_0 [R]^T \omega^2 \{u\} \tag{6}$$

The modal properties of the structure in air, i.e. natural frequencies and mode shapes, are obtained from Equation (3) taking the vector $\{p\} = 0$ on the hydrofoil surface. The modal properties of the structure surrounded by water are obtained by solving the coupled solution of Equations (3) and (4). The acoustic modes of the surrounding water domain inside the test section cavity are solved with Equation (6) and taking $\{u\} = 0$ on the hydrofoil surface. For simplicity, the surrounding fluid is assumed to be homogeneous which is a reasonable assumption for many uniformly mixed gas-liquid flows.

3 Validation of the numerical model

The experimental conditions comprised a 2D NACA0009 hydrofoil with a chord of 0.1 m, a span of 0.15 m and a truncated trailing edge with a thickness of 0.00322 m. The hydrofoil was made of aluminum with a density of 2700 kg/m^3, a Young's modulus of 52 GPa and a Poisson's ratio of 0.3. The hydrofoil was mounted inside the tunnel test section with an incidence angle of 0º in the position indicated on the top view plotted in Figure 2a. The test section dimensions were 0.15×0.15×0.885 m^3. The acoustic properties of the surrounding water were considered homogeneous with a density of 1000 kg/m^3 and a speed of sound of 1450 m/s.

All the test section boundaries in the fluid domain were set as fully reflective with the exception of the inlet and outlet surfaces that were defined as absorbing boundary conditions with an absorption coefficient of 0.3. Since the hydrofoil was clamped inside the test section and a small gap of 0.00012 m existed between its free lateral surface and the test section wall, a thin layer of fluid elements was created to model such condition.

The hydrofoil natural frequencies and mode shapes were extracted from the amplitudes of vibration of 26 points measured by a Laser Doppler Vibrometer on the hydrofoil surface as indicated in Figure 2b. Different fluid conditions including the hydrofoil in air and in still water were tested. The hydrofoil modes of vibration were mechanically excited by two PZT patches. As a result, the three first modes of vibration were identified and characterized which comprised the first bending (fs_1), the first torsion (fs_2) and the second bending (fs_3) modes. The corresponding mode shapes obtained with the numerical model in air are shown

on the first column in Table 2.

To check the accuracy of the model, the deviations between simulated and measured natural frequencies for the three modes are indicated in Table 1. As it can be seen, all the deviations are below 9%. Furthermore, the experimental and numerical mode shapes are compared for the three modes from Figures 3 to 5, respectively, in air and in water. It can be confirmed that the relative amplitudes of the hydrofoil deformations obtained numerically are close to the measured ones. Although some points can present larger deviations, the general trend of the curves is consistent. In conclusion, it can be stated that the coupled acoustic fluid-structure model is an accurate tool that can be used to predict the hydrofoil dynamic behavior surrounded by air or water.

4 Coupled system modes induced by acoustic modes

Although the calculated frequencies and mode shapes for fs_1, fs_2 and fs_3 agreed well with experimental results both in air and in water, additional modes were predicted in water when the coupled system was solved. In Table 2, the first four natural frequencies are indicated with their mode shapes for the actual tunnel test section dimensions (called long cavity model). As it can be seen, an intermediate mode around 816 Hz was predicted between the 1st torsion fs_2 and the 2nd bending fs_4 with transverse deformation.

In fact, this vibration was induced on the hydrofoil by an acoustic mode of the water cavity. This was demonstrated by the fact that this mode disappeared when the dimensions of the test section and the rest of model parameters were kept constant. Particularly, when the length of the tunnel test section was decreased from 0.885 m to 0.300 m (called short

cavity model), a new set of modes was obtained that is indicated in Table 2. In that case the third mode was the 2nd bending mode fs_3.

If the results of the long and the short cavities models shown in Table 2 are compared, it can be concluded that there are two types of modes:

- a set of modes with equal natural frequencies and mode shapes between the two cavity sizes, such as fs_1, fs_2, fs_4 for the long cavity model and fs_1, fs_2, fs_3 for the short cavity model.

- a set of modes with natural frequencies dependent on the cavity size, such as fs_3 for the long cavity model.

The fs_3 for the long cavity model presented the main structure deformation along the hydrofoil mean plane in transverse direction (horizontal) and with lower amplitudes than for the rest of modes. The maximum deformation was located at the free tip section. It must be noted that this mode was not detected during the experiments, which corresponds to the long cavity case, because the displacements in such direction were not measured. Therefore, fs_3 is a mode of vibration that could be induced by a pure acoustic resonance according to Parker's studies. In the following sections, the appearance of induced hydrofoil modes due to coupling with acoustic modes has been analyzed in more detail.

5 Influence of cavity dimensions and speed of sound on coupled modes

The seven first acoustic modes of the long and the short cavity domains were calculated with the hydrofoil surface displacement restrained to zero, $\{u\} = 0$, and Equation (4) for speeds of sound from 1450 m/s down to 10 m/s. All the acoustic frequency values, ff, were

normalized using the hydrofoil chord length, C, and the reference speed of sound, $c_0 = 1450$ m/s, with Equation (7).

$$f^* = ff \times C / c_0 \tag{7}$$

The corresponding normalized frequencies, f^*, have been plotted in Figure 6 as a function of the speed of sound ratio c_f / c_0. The acoustic frequencies of the long cavity have been plotted with dotted lines, meanwhile the frequencies of the short cavity have been presented with continuous lines. The corresponding mode shapes have also been plotted on the left hand side of Figure 6 for the short cavity and on the right hand side for the long cavity.

It can be observed that all the frequencies decrease linearly as the speed of sound decreases while the mode shapes remain exactly the same. This is can be explained with Equation (6) because the acoustic fluid mass matrix term increases as the speed of sound decreases and the $\left[\bar{M}_f \right]$ keeps constant. In additions, the acoustic frequencies of the short cavity are higher than the frequencies of the long cavity as expected. Another observation is that the order of the mode shapes is different between the short and the long cavity cases. Mode shape correspondence is only observed in the following cases:

- Mode shape ff_3 for the long cavity $\equiv$ Mode shape ff_1 for the short cavity;

- Mode shape ff_5 for the long cavity $\equiv$ Mode shape ff_2 for the short cavity;

- Mode shape ff_7 for the long cavity $\equiv$ Mode shape ff_3 for the short cavity.

Since the intrinsic structure modes are not greatly affected by the size of the fluid domain, the short cavity fluid domain with dimensions 0.15×0.15×0.300m was used in the following analysis without hindering the conclusions.

6 Coupling behavior between acoustic and structure mode

The normalized values of the coupled system natural frequencies f^* have been plotted in Figure 7 as a function of c_f/c_0 for the two cavity sizes. The trends followed by the structure modes, fs, are represented with continuous lines , meanwhile the trends of the acoustic modes, ff, are represented with dotted lines. The continuous lines with the same color also correspond to the order of appearance of the coupled modes for each sound speed condition. The black one represents the lowest frequency mode and then the following ones are the red, the blue, the pink and so on. For example, the results shown at $c_f/c_0 = 1.0$ in Figure 7a correspond to the modes presented in Table 2 for the long cavity and those in Figure 7b correspond to the short cavity. As previously observed, the three first modes for the short cavity correspond to the three first structure modes but for the long cavity the third mode, f_{s3}, corresponds to an acoustic mode.

From these plots it can be observed that the natural frequencies of the structure modes and their order of appearance are not affected by the reduction of the speed of sound until an acoustic mode crosses them. Then, two possible couplings can take place as described in Sections 6.1 and 6.2. On the one hand, a strong coupling between the structure mode and the acoustic mode occurs and they become a single coupled mode which frequency decreases linearly with c_f. On the other hand, a new coupled mode appears with a frequency that decreases linearly with c_f but the structure mode keeps the mode shape and the constant frequency.

6.1 First type coupling modes

The first coupling mechanism occurs between the acoustic and the structure modes with similar mode shapes. Under such conditions the pressure distribution induced by the acoustic mode matches the hydrofoil deformation induced by the structure mode.

Among the acoustic modes for the short cavity (left hand side of Figure 6), the ff_2, ff_6 and ff_7 present mode shapes that can enhance the bending and torsion deformations of the hydrofoil. They are the modes that present pressures with opposite signs on the top and the bottom surfaces of the hydrofoil and that keep the symmetry of the absolute pressure values across the horizontal plane passing through the chord. Their natural frequencies have been plotted in Figure 8a, 8b and 8c as a function of sound speed. The pressure distribution on the hydrofoil surface has also been plotted in the same figures, as well as the displacement of the hydrofoil surface under the structure mode that fits better the acoustic pressure distribution.

In Figure 8a, it can be clearly seen that when $0.1 < c_f/c_0 < 1.0$, the natural frequency of the 1st bending mode is constant and it is not affected by the sound speed. When $c_f/c_0 < 0.1$, the natural frequency of the 1st bending structure mode, fs_1, approaches the acoustic mode ff_2. Then, the natural frequency of the 1st bending structure mode, fs_1, starts to decrease and and joins the acoustic mode. In fact, they merge and keep coupled for the rest of lower sound speeds because the acoustic effect is stronger than the FSI effect. In Figures 8b and 8c the same behavior can be observed for the couplings between ff_6 and f_{s2} and between ff_7 and f_{s3}, respectively. In conclusion, when the shape of an acoustic mode resembles the shape of a structure mode, they will become a strong coupled mode.

6.2 Second type coupling modes

The acoustic modes ff_1, ff_3 and ff_4 of the short cavity provoke pressure distribution on the hydrofoil surface that do not match any of the surface displacements of the three first structure modes of vibration.

For example, the frequency of fs_2 (red line in Figure 7b) is constant when $0.25 < c_f/c_0 < 1.0$. At this point, the structure mode of vibration crosses the first acoustic mode of vibration ff_1 (green dotted line). Then, a new coupled system mode appears and its frequency decreases linearly following the constant slope observed for the acoustic mode. This behavior is called "mode transition" because it occurs between two consecutive structure modes with different mode shapes.

Several points (A to F) have been selected in Figure 9 to show the first mode transition with three crossings. The first transition takes place at point A, the second at point C and the third at point E. The mode shapes at points C_1 (fs_2) and C_2 (fs_3) located to the right and to the left of the mode transition point C, respectively, are shown in Figure 9. They correspond to the 1st torsion mode and they have the same vibration amplitude as in pure water (see Table 2).

On the other hand, the mode shapes at points A, B, C, D, E and F of the coupled mode of vibration during the mode transition are exactly the same. They present a shrinking and stretching motion along the stream wise direction which is different from any of the original structure mode shapes for a fully wetted hydrofoil with $c_f/c_0 = 1.0$ (shown on the right of Figure 9). Obviously, this mode shape is induced by the ff_1 mode of vibration shown on the

top left of Figure 9. Figure 10 represents the second mode transition line. Another new mode shape of the coupled system appears from point I to point N corresponding to a forward and backward movement in span wise direction. Again, this mode shape is induced by the third acoustic modes (ff_3). So it can be concluded that it is the additional acoustic mode in the span wise fluid acoustic mode which produces the new structure mode shapes and causes the transfer of structure modes. All the transition points are on the locations where the acoustic frequency is close to structure mode under $c_f/c_0 = 1.0$ condition. On the transition line the structure frequency and mode shape corresponds to the acoustic mode. It is also found that the coupled mode along the transition line caused by acoustic mode has a relative small magnitude of 10^{-7} compared with the basic structure mode.

Based on the previous observations, the different coupled system modes obtained with the two different fluid domain dimensions shown in Table 2 can be explained. More mode transition lines can be found with the long cavity domain than with the short cavity domain because for the longer one the acoustic frequencies are lower and they can interact more times with the structure frequencies. For the long domain, the lowest acoustic mode ff_1 corresponds to a stream wise mode shape analogous to the ff_1 for the short domain except that the frequency is much lower. As a result, an additional structure mode corresponding to ff_1 appears with the long domain between the torsion mode and the second bending mode (see Figure 7a). As it can be seen in Table 2 for mode f_{s3}, this additional mode is stream wise as the first acoustic mode ff_1.

7 Conclusions

An acoustic coupled fluid-structure numerical model was developed and validated to simulate the dynamic behavior of a NACA0009 hydrofoil inside a water tunnel test section surrounded by air and still water. The calculated results in terms of natural frequencies and mode shapes of the first bending, the first torsion and the second bending modes presented a good agreement with experimental results. Then, the validate model was used to simulate the effect of the test section dimensions and of the speed of sound in water.

It was found that reducing the distance of the tunnel test section walls to the hydrofoil increased the acoustic frequencies of the water domain. Moreover, the reduction of the sound speed provoked a linear reduction of all the acoustic frequencies. On the other hand, the hydrofoil frequencies were not affected by the change of sound speed except when they were coupled with an acoustic frequency. Then, two different behaviors were identified.

If the acoustic mode shape had a pressure distribution similar to the hydrofoil deformation, both modes suffered a strong coupling and evolved together with a linear decrease of frequency with the sound speed. If the mode shapes were dissimilar, then a new fluid-structure mode appeared that followed the linear reduction of the acoustic mode which appeared as a mode transition between two consecutive hydrofoil modes. As a result, with the reduction of sound speed several mode transitions could be plotted that evolved between the intersections of the diagonal acoustic mode lines and the horizontal hydrofoil mode lines.

In summary, it has been found that the dimensions and the speed of sound inside the water tunnel test section have a great influence on the hydrofoil coupled modes of vibration.

Therefore, they should be taken into account when using high-speed water tunnels for experimental and numerical research.

Acknowledgment

References

[1] Lindholm, U., Kana, D., Chu, W., Abramson, H. and Norman, H., 1965. Elastic vibration characteristics of cantilever plates in water. Journal of Ship Research, 9, pp. 11-29.

[2] Meyerhoff, W., 1970. Added masses of thin rectangular plates calculated from potential theory. Journal of Ship Research, 2, pp. 100-111.

[3] Kwak, M.K., 1991. Vibration of circular plates in contact with water. Journal of Applied Mechanics, 58(2), pp. 480-483.

[4] Amabili, M., 1996. Free vibration of partially filled, horizontal cylindrical shell. Journal of Sound and Vibration, 191(5), pp. 757-780.

[5] Chang, T., and Liu, M., 2000. On the natural frequency of a rectangular isotropic plate in contact with fluid. Journal of Sound and Vibration, 236(3), pp. 547-553.

[6] Rodriguez, C. G., Egusquiza, E., Escaler, X., Liang, Q. W., and Avellan, F., 2006. Experimental investigation of added mass effects on a Francis turbine runner in still water. Journal of Fluids and Structures, 22(5), pp. 699-712.

[7] Valentín, D., Presas, A., Egusquiza, E. and Valero, C., 2014. Experimental study on the

added mass and damping of a disk submerged in a partially fluid-filled tank with small radial confinement. Journal of Fluids and Structures, 50, pp. 1-17.

[8] Escaler, X., and De La Torre O. 2018. Axisymmetric Vibrations of a Circular Chladni Plate in Air and Fully Submerged in Water. Journal of Fluids and Structures, 82, pp. 432–445.

[9] Parker, R., 1966. Resonance effects in wake shedding from parallel plates: Some experimental observations. Journal of Sound and Vibration, 4(1), pp. 62–72.

[10] Parker, R., and Llewelyn, D., 1972. Flow induced vibration of cantilever mounted flat plates in an enclosed passage: an experimental investigation. Journal of Sound and Vibration, 25(3), pp. 451-463.

[11] Parker, R., and Stoneman, S. A. T., 1989. The excitation and consequences of acoustic resonances in enclosed fluid flow around solid bodies. Proceedings of the Institution of Mechanical Engineers, Part C: Mechanical Engineering Science, 203(1), pp. 9-19.

[12] Woodley, B. M., and Peake, N., 1999. Resonant acoustic frequencies of a tandem cascade. part 1. zero relative motion. Journal of Fluid Mechanics, 393, pp. 215-240.

[13] Bardakhanov, S. P., and Belai, O. V., 2000. Excitation of subharmonic oscillations in an axisymmetric flow with coherent structures in the regime of aeroacoustic resonance. Journal of Applied Mechanics and Technical Physics, 41(4), pp. 628-636.

[14] Konig, S., and Petry, N., 2012. Parker-Type acoustic resonances in the return guide vane cascade of a centrifugal compressor-theoretical modeling and experimental verification. Journal of Turbomachinery-Transactions of the ASME, 136(6), pp. 061029.

[15] Bossio, M., Valentín, D., Presas, A., Martin, D. R., Egusquiza, E., Valero, C., and

Egusquiza, E., 2017. Numerical study on the influence of acoustic natural frequencies on the dynamic behaviour of submerged and confined disk-like structures. Journal of Fluids and Structures, 73, pp. 53-69.

[16] Blevins, R. D., 2001. Formulas for Natural Frequency and Mode Shape. Krieger Publishing Company.

[17] Brennen, C.E., 1995. Homogeneous Bubbly Flows, Cavitation and Bubble Dynamics. Oxford University Press, Oxford.

[18] De La Torre, O., Escaler, X., Egusquiza, E. and Farhat, M., 2014. Numerical and experimental study of a nearby solid boundary and partial submergence effects on hydrofoil added mass. Computers & Fluids, 91, pp. 1-9.

[19] De La Torre, O., Escaler, X., Egusquiza, E., and Farhat, M., 2013. Experimental investigation of added mass effects on a hydrofoil under cavitation conditions. Journal of Fluids and Structures, 39, pp. 173-187.

[20] De La Torre, O., Escaler, X., Egusquiza, E., and Farhat, M., 2016. Experimental mode shape determination of a cantilevered hydrofoil under different flow conditions. Proceedings of the Institution of Mechanical Engineers Part C Journal of Mechanical Engineering Science, 230(5), pp. 3408-3419.

[21] Liu, X., Zhou, L., Escaler, X., Wang, Z., Luo, Y., and De La Torre, O., 2017. Numerical simulation of added mass effects on a hydrofoil in cavitating flow using acoustic FSI. Journal of Fluids Engineering, 139(4), pp. 041301.
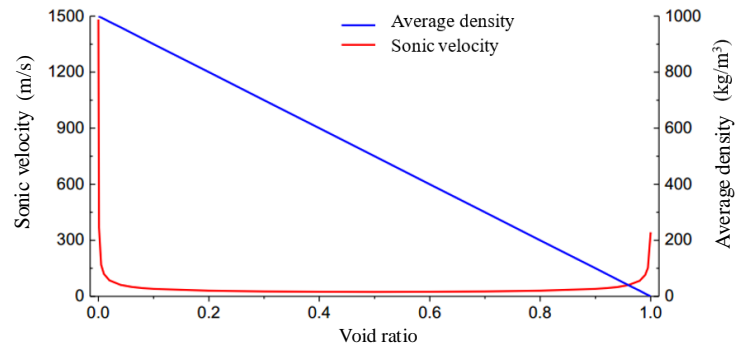
Figure Captions List

Figure 1   Speed of sound (red line) and cavity density (blue line) as a function of void ratio in a bubbly air/water mixture at atmospheric pressure.
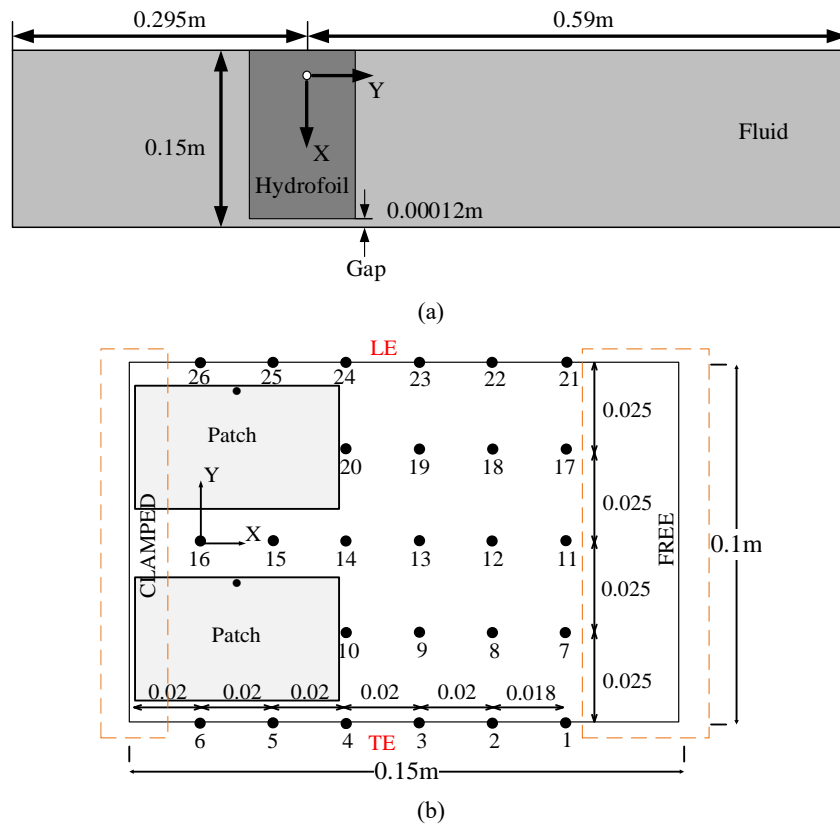
Figure 2   Top view of the computational domain (a); top view of the hydrofoil surface and measurement points [LE = leading edge, TE = trailing edge] (b)[20].
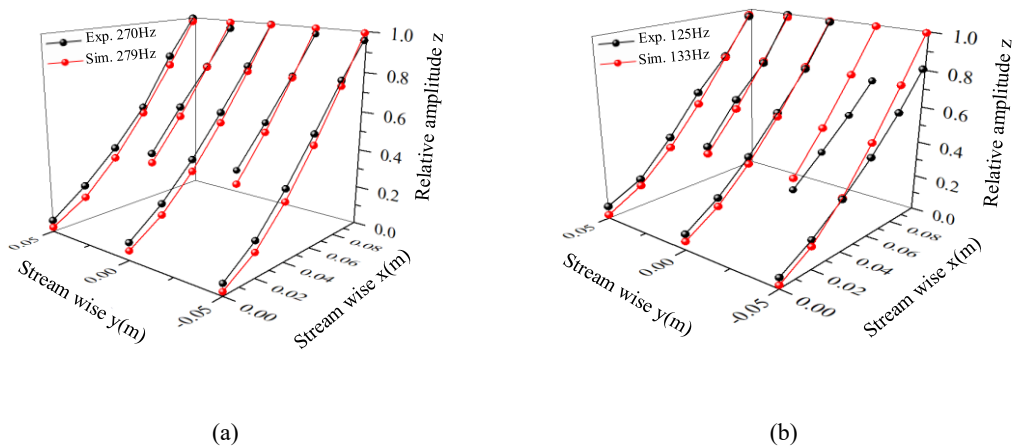
Figure 3   Comparison of numerical and experimental mode shapes for fs_1 in air (a) and still water (b).
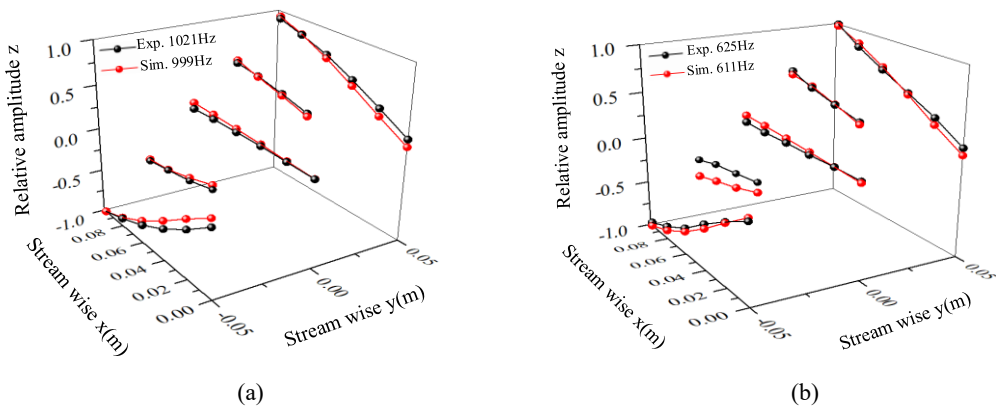
Figure 4   Comparison of numerical and experimental mode shapes for fs_2 in air (a) and still water (b).
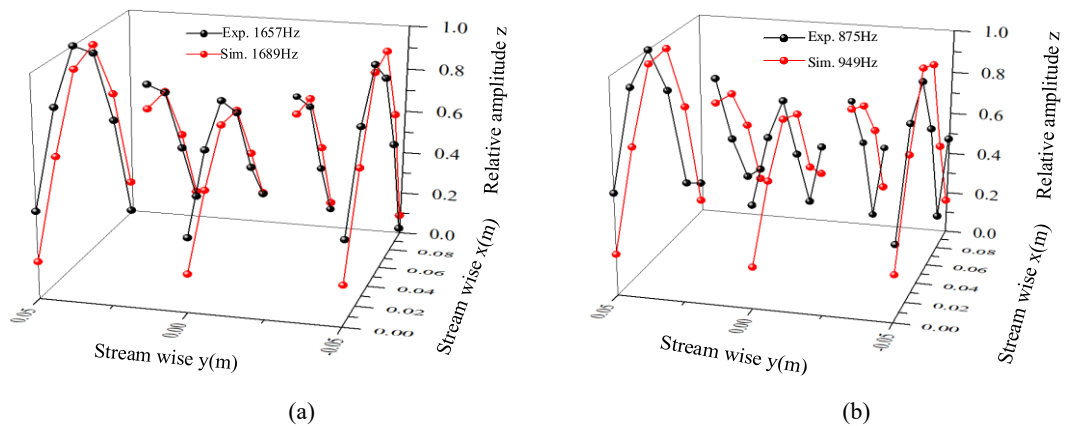
Figure 5   Comparison of numerical and experimental mode shapes for fs_3 in air (a) and still water (b).
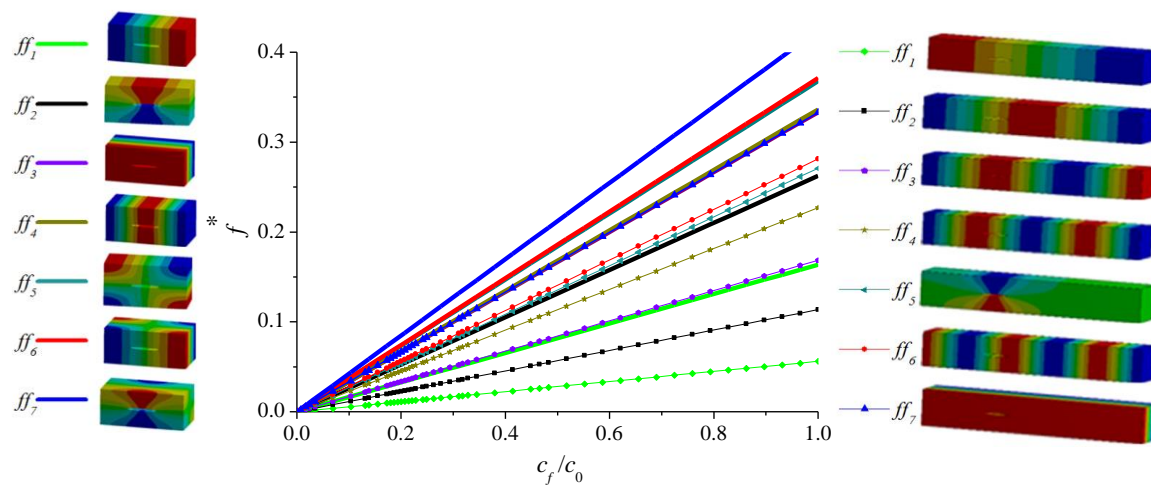
Figure 6   Natural frequencies and mode shapes of the seven first acoustic modes of the water cavity as a function of the speed of sound for a long domain (right hand side plots and dotted lines) and for a short domain (left hand side plots and continuous lines).
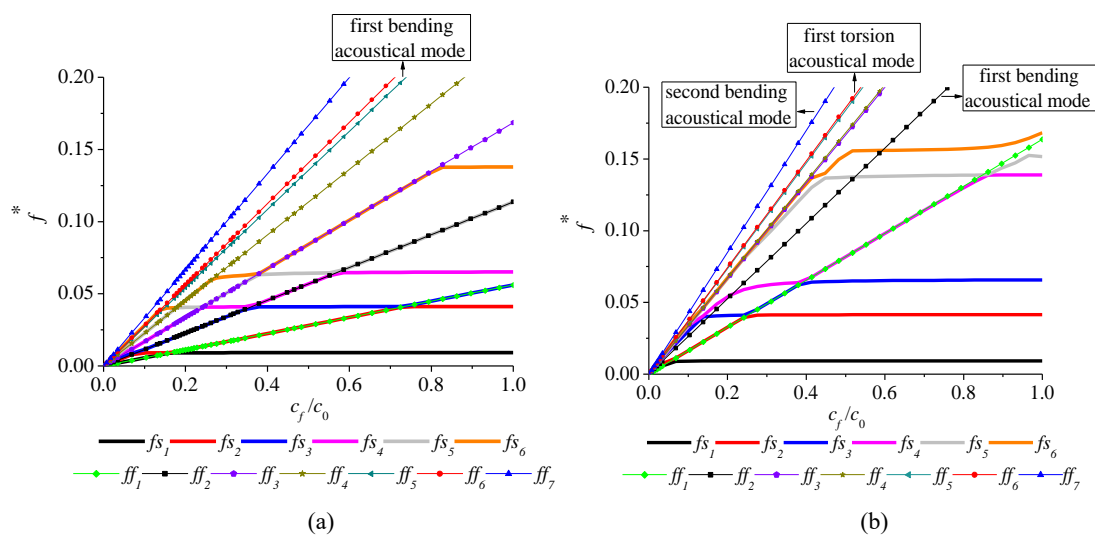
Figure 7   Natural frequencies of the six first hydrofoil modes and of the seven first acoustic modes of the water domain as a function of the speed of sound ratio for the long (a) and the short (b) domains.
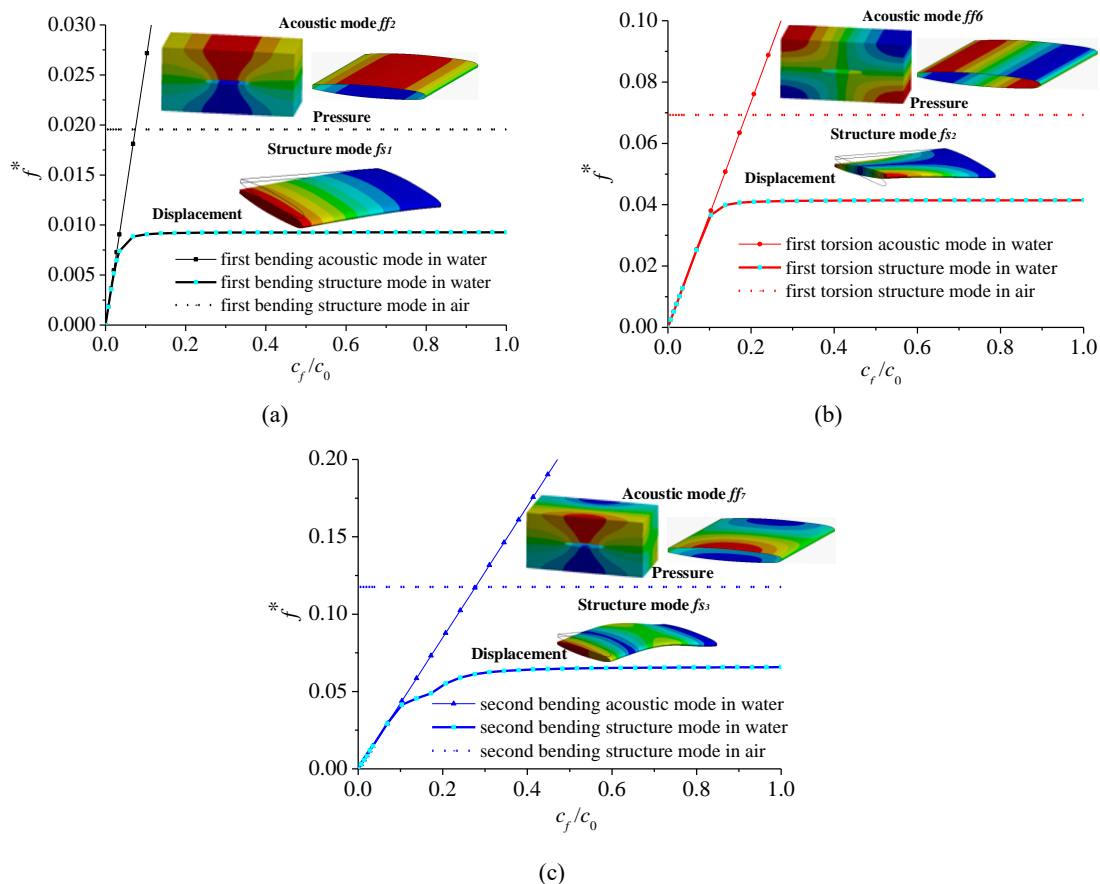
Figure 8   Evolution of the natural frequencies as function of c_f for acoustic and structure modes with similar mode shapes: ff_2 vs fs_1 – 1st bending - (a), ff_6 vs fs_2 - 1st torsion - (b), and ff_7 vs fs_3 – 2nd bending – (c).
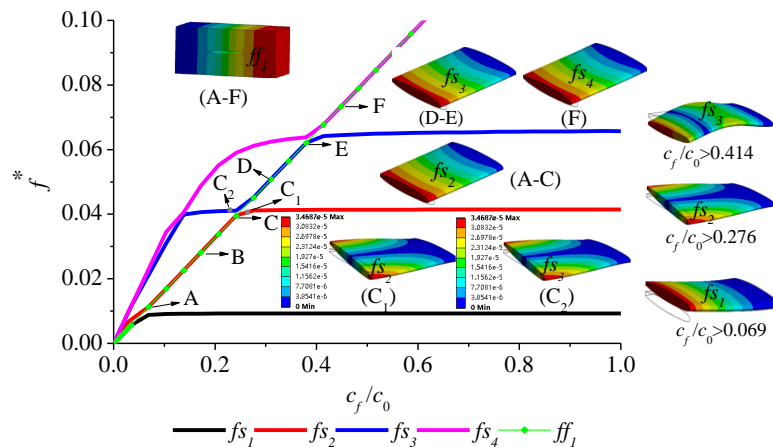
Figure 9   First mode transition line with varying c_f.

Figure 10   Second mode transition line with varying c_f.

Table Caption List

Table 1   Experimental and numerical hydrofoil natural frequencies in air and in still water, and percent deviations.

Table 2   Simulated modes in air and in water for the long cavity (actual test section size of the cavitation tunnel) and for the short cavity (fictitious size).

Figure 1. Speed of sound (red line) and cavity density (blue line) as a function of void ratio in a bubbly air/water mixture at atmospheric pressure.

(a)

(b)

Figure 2. Top view of the computational domain (a); top view of the hydrofoil surface and measurement points [LE = leading edge, TE = trailing edge] (b) [20].

(a)   (b)

Figure 3. Comparison of numerical and experimental mode shapes for fs_1 in air (a) and still water (b).

(a)   (b)

Figure 4. Comparison of numerical and experimental mode shapes for fs_2 in air (a) and still water (b).

(a)   (b)

Figure 5. Comparison of numerical and experimental mode shapes for fs_3 in air (a) and still water (b).

Figure 6. Natural frequencies and mode shapes of the seven first acoustic modes of the water cavity as a function of the speed of sound for a long domain (right hand side plots and dotted lines) and for a short domain (left hand side plots and continuous lines).

Figure 7. Natural frequencies of the six first hydrofoil modes and of the seven first acoustic modes of the water domain as a function of the speed of sound ratio for the long (a) and the short (b) domains.

(a)

(b)

(c)

Figure 8. Evolution of the natural frequencies as function of c_f for acoustic and structure modes with similar mode shapes: ff_2 vs fs_1 – 1st bending - (a), ff_6 vs fs_2 - 1st torsion - (b), and ff_7 vs fs_3 – 2nd bending – (c).
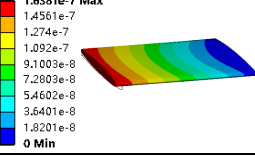
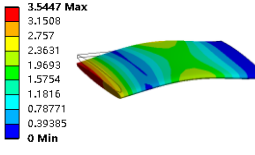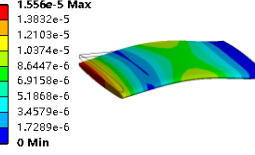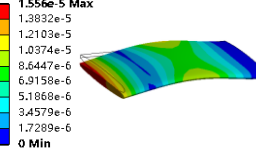**Figure 9.** First mode transition line with varying c_f.

Figure 10. Second mode transition line with varying c_f.

Table 1. Experimental and numerical hydrofoil natural frequencies in air and in still water, and percent deviations.

Mode	First bending f_1		Torsion f_2		Second bending f_3	
Conditions	Air	Water	Air	Water	Air	Water
Exp. [Hz]	270	125	1021	625	1657	875
Sim. [Hz]	279	133	999	611	1689	949
Dev. [%]	3.5	6.6	2.1	-2.2	1.9	8.4

Table 2. Simulated modes in air and in water for the long cavity (actual test section size of the cavitation tunnel) and for the short cavity (fictitious size).

Air	Water		Mode Shapes
	Long Cavity (actual size)	Short Cavity	
f_1 = 279 Hz	fs_1 = 133 Hz	fs_1 = 134 Hz	1st bending (fs_1)
f_2 = 999 Hz	fs_2 = 611 Hz	fs_2 = 612 Hz	1st torsion (fs_2)
	fs_3 = 816 Hz		
f_3 = 1689 Hz	fs_4 = 949 Hz	fs_3 = 950 Hz	2nd bending (fs_3)